J Appl Electrochem (2013) 43:619–628
DOI 10.1007/s10800-013-0549-y

ORIGINAL PAPER

Pulsed and potentiostatic electrodeposition of $CuInSe_2$ on gold-coated alumina substrates

M. Valdés · M. Mollar · M. Vázquez · B. Marí

Received: 29 January 2013 / Accepted: 6 April 2013 / Published online: 20 April 2013

Abstract $CuInSe_2$ thin films were deposited on gold-coated alumina electrodes using constant and pulsed potential signals. In situ electrochemical measurements were recorded with an atomic force microscope to follow $CuInSe_2$ electrodeposition. The electrodeposited films were characterized employing scanning electron microscopy, energy dispersive spectroscopy, grazing incidence X-ray diffraction, and Raman spectroscopy. The best stoichiometry is attained for films deposited at pulsed potentials of −0.7 V. These films are also the most compact, showing a homogeneous morphology. In contrast, potentiostatic films presented minor variations in their chemical composition with the deposition potential. The morphology presented porous coral-like structures. X-ray and Raman spectroscopy analysis of as-deposited films by either technique reveal the presence of secondary phases such as Cu_xSe and Se, especially at the most positive deposition potentials. After a thermal treatment at 500 °C in Se vapor, the crystallinity of the material is significantly enhanced and no secondary phases are present.

Keywords $CuInSe_2$ · Semiconductor · Thin films · Electrodeposition · AFM

M. Valdés (✉) · M. Vázquez (✉)
División Electroquímica y Corrosión, INTEMA, Facultad de Ingeniería, CONICET-Universidad Nacional de Mar del Plata, Juan B. Justo 4302, B7608FDQ Mar del Plata, Argentina
e-mail: mvaldes@fi.mdp.edu.ar

M. Vázquez
e-mail: mvazquez@fi.mdp.edu.ar

M. Mollar · B. Marí
Departament de Física Aplicada – IDF, Universitat Politècnica de València, Camí de Vera s/n, 46022 Valencia, Spain

1 Introduction

$CuInSe_2$ (CISe) is one of the most extensively investigated materials in the field of thin film solar cells. Due to its outstanding optical properties and chemical stability, this is a suitable material to be used in thin film solar cells.

Cost-effective solar cells are crucial to achieve massive thin film photovoltaic production. Low-price and non-vacuum deposition techniques are key strategies to reduce costs [1]. Among them, electrodeposition presents important advantages: it can produce coatings over large areas, it can copy intricate geometries, and it can be used in combination with various kinds of substrates [2]. Direct electrodeposition of $CuInSe_2$ has led to the production of solar cells with competitive cell efficiencies close to 12 % [3] and there are several companies that are currently producing solar cells based on electrodeposited CISe [4].

For these reasons there is permanent interest in the electrodeposition process, so as to understand the complex mechanisms involved in CISe electroplating, taking into account the many parameters involved [5, 6].

Electrodeposition can be performed at a fixed potential or current (potentiostatic or galvanostatic). Alternatively, the potential or current can be applied using pulses or alternating signals [7]. In the particular case of CISe electrodeposition, there are several publications that include a mechanistic approach to CISe formation, but most of them focus on electrodeposition at fixed potential [8–11]. It has been well established that, if the precursor electrolyte contains indium in excess, the composition of the film is controlled by the ratio between selenium and copper fluxes (J) arriving at the electrode surface. This parameter is called α and is defined as $\alpha = J_{Se(IV)}/J_{Cu(II)}$.

For pulsed electrodeposition, there are a few articles where the mechanistic aspects have been discussed

[12, 13]. Considering the profile of the alternating signal imposed on the electrode, it can be expected that the experimental parameters (such as substrate and electrolyte composition, potentials, and times among others) will play a different role in the mechanism.

In previous publications, we have evaluated the influence of the deposition potential [14] and deposition time [15] in potentiostatic and pulsed CISe films deposited on conductive glass (TCO). In those cases, α was set as 2 in the precursor electrolyte. An excess in the Se content has been observed in the CISe films prepared by pulsed electrodeposition. For this reason in the present study, α has been set at 1.5.

The changes in structure, morphology, and composition produced when the potential is pulsed are evidenced by comparison with CISe thin films electrodeposited at constant potential. Moreover, this investigation incorporates in situ atomic force microscopy (AFM) to explore the first stages of $CuInSe_2$ electrodeposition, providing valuable information on the films growth as a function of potential.

2 Experimental aspects

2.1 Electrochemical techniques and electrodeposition of $CuInSe_2$ films

Al_2O_3 substrates were coated with a thin film of gold ($\sim$100 nm) by dc sputtering. Prior the deposition the substrates were ultrasonically cleaned in acetone and ethanol. CISe electrodeposition was performed at room temperature in a conventional three-electrode electrochemical cell. The precursor electrolyte consisted of an aqueous solution containing 2 mmol dm^{-3} $CuCl_2$, 8 mmol dm^{-3} $InCl_3$, and 3 mmol dm^{-3} SeO_2 with 0.1 mol dm^{-3} LiCl as supporting electrolyte (Cu:In:Se ratio resulted in 1:4:1.5). The pH was adjusted to 2 with a few drops of a concentrated HCl stock solution. Before each electrodeposition, argon was bubbled through the solution to remove dissolved oxygen. During the electrodeposition the solution was softly stirred using a magnetic stirrer. The Al_2O_3/Au substrate serves as the working electrode (active area $\sim$1.4 cm^{-2}), complemented by a Pt wire as counter-electrode, and a Ag/AgCl/KCl sat. as a reference electrode (+0.21 V vs. SHE). Electrodepositions were performed employing a Keithley 2602 system sourcemeter operated with in-home developed software.

Pulsed electrodeposition (Pulsed) of CISe films was carried out using a square-pulse voltage, with a step defined between two potential values (E_1 and E_2). To investigate the effect of the potential, E_1 was varied between -0.4 and -0.7 V while E_2 was kept constant at a fix value of 0.0 V in all the films. The effect of using different E_2 values was out of the scope of this study, although it was found that E_2 positive to 0.0 V resulted in film detachment. This variable has been investigated by Hu et al. [13], who showed that the Cu/In ratio was influenced by changing the reverse voltages. The duration of each potential step was 10 s for both, E_1 and E_2, resulting in a duty cycle of 50 %.

For the sake of comparison, potentiostatic (Pot) CISe films were deposited at three different values of cathodic potentials: -0.5, -0.6, and -0.7 V. In order to obtain films with similar thicknesses, pulsed and potentiostatic CISe films were deposited until a final electrochemical charge of 4 C was achieved. On average, 1,500 s and 100 cycles (2,000 s) were necessary to achieve this charge for Pot and Pulsed CISe films, respectively. After completing the deposition, the deposited films were gently rinsed with distilled water and dried in air. Later, the films were selenized in a tube furnace. The samples were placed for 30 min in a graphite cylinder together with Se pellets ($\sim$0.1 g). The temperature and heating rate of the thermal treatment were set at 500 °C and 10 °C min^{-1}, respectively. Argon was employed as gas carrier. After selenization, CISe films were let to cool inside the tube.

In situ Atomic Force Microcopy images were obtained using a Multimode AFM (Digital Instruments VEECO Methodology Group, USA) with a NanoScope IIIa controller and equipped with a J-type scanner. The topography of the samples was studied in contact mode. An oxide-sharpened silicon nitride probe has been used with a V-shaped cantilever configuration. To perform electrochemical measurements, an electrochemical-AFM (EC-AFM) package included an electrochemical cell which could be mounted on the AFM and coupled to a Digital Instruments universal bipotentiostat (VEECO Methodology Group). More details of the EC-AFM set-up can be found elsewhere [16]. This three-electrode AFM-electrochemical cell was used to collect images during cyclic voltammograms. First, gold was sputtered on a mica tape to obtain a highly smooth surface. Then this tape was glued on a metallic disk and finally the mica tape was removed leaving a gold deposit on the disk. These disks were used as working electrodes in the AFM cell, where two platinum wires were employed as reference and auxiliary electrodes. During these experiments, the potential was measured against Pt (+0.35 V vs. Ag/AgCl). The coupled AFM-electrochemical experiments were performed after placing 500 μL of the precursor solution for the electrodeposition of $CuInSe_2$ films on top of the disks. Cyclic voltammetry was performed sweeping the potential, from +0.3 to -1.3 V_{Pt}, at a scan rate of 5 mV s^{-1}.

2.2 Thin films characterization

The morphology and the chemical composition of the films were registered with a scanning electron microscope (JEOL-JSM6300) coupled with an X-ray microanalysis

system (Link-Oxford-Isis). The crystalline structure of the films was analyzed by X-ray diffraction in grazing incidence configuration (GXRD) using a PANalytical X'Pert PRO diffraction system employing Cu-Kα radiation at 40 kV and 40 mA. The samples were scanned between 15° and 75° with a step size of 0.01°. The crystallographic data for each phase were taken from the literature [17]. Raman spectroscopy measurements were performed using an Invia Reflex confocal Raman microprobe using a 100× objective. Excitation was provided with the 514 nm emission line of an Ar^{+} laser. Using neutral density filters, the power of the laser was reduced to 10 % to prevent damage by heating. Raman micro-mapping was performed scanning a square zone (40 × 40 μm) in the sample and recording 25 spectra in the x and y directions. For both axes the step between spectra was set in 10 μm.

3 Results and discussion

3.1 In situ electrochemical-AFM study

Figure 1 shows the cyclic voltammogram (CV) obtained using the precursor CISe solution during in situ-AFM measurements with gold-coated alumina as substrate. The shape of the curve is in agreement with previous studies carried out on Mo foils by Marí and co-workers [18]. During the first cycle, the first cathodic current peak appears at 0.1 V, which can be related to the reduction of Cu^{+2} ions. The second cathodic peak is located between 0 and −0.25 V. This peak can be associated to the deposition of secondary phases such as Cu_xSe and/or Se, especially at low deposition potentials (about −0.20 V) that normally

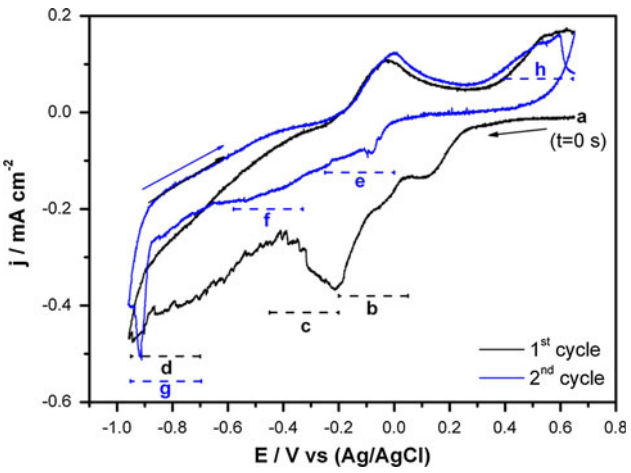

Fig. 1 Cyclic voltammogram of the CISe solution precursor recorded during AFM measurements. The scan rate was 5 mVs^{-1}. The *arrows* denote the direction of the potential scan. *Dashed segments*, labeled with letters, indicate the potential ranges where topographic images were taken (see Fig. 2)

precedes the formation of CISe films [9, 19]. During the second cycle the current values registered are lower than in the first one, probably because the electrode is partially covered by a resistive deposit. The current increment observed around −0.7 V can be associated to the Se^{+4} reduction to Se^{-2} and the subsequent $CuInSe_2$ deposition.

Topographic 3D images were taken in situ as the potential imposed on the gold electrode was being swept. These images are shown in Fig. 2. Figure 2a displays the topography of the electrode surface at open circuit potential, before starting the potential scan. As it was mentioned above, the electrodeposition of CISe films is preceded by the deposition of Cu_xSe compounds. The topographic image taken during the potential sweep from 0.14 to −0.2 V (Fig. 2b) confirms the deposition and growth of a solid phase within the same potential range where the current shows a peak at the voltammogram. At more negative potentials, the amount of solids deposited on the surface increases (Fig. 2c, d) and the material appears to nucleate showing pyramidal features. This has been previously reported for Cu electrodeposition in acidic media [20].

The morphology of the electrode at the negative end of the first cycle is presented in Fig. 2d. During the second scan (Fig. 2e, f) a rougher surface is observed, mainly formed by bigger pyramidal structures as a consequence of the continuous deposition on the electrode. Figure 2e still shows sharp peaks probably related to the formation of some Cu_xSe phases. At more negative potentials (Fig. 2f, g) the peaks become softer and the deposition rate rises due to the formation of CISe.

It is normally found that after the first cycle in a cyclic voltammogram, the deposition initiates at more anodic potentials in the subsequent scans. This phenomenon has been explained by the fact that the residual layer previously deposited is providing active sites so that the subsequent discharge of new ions requires less energy [21]. At higher negative potentials the roughness still increases but the small nodular features are replaced by valleys, as observed in Fig. 2g, h. This can be related to particle agglomeration, which is frequently seen in electrodeposited CISe films after long deposition times.

3.2 Electrochemical deposition

Figure 3 compares the evolution in time of the potential and the current density for potentiostatic (Fig. 3a) and pulsed (Fig. 3b) electrodeposition. When the potential is constant, the current decays as soon as the potential is imposed, probably due to the change in the precursor's concentration when the ions close the electrode surface start to react. Later, the current attains a limiting value, typical of a deposition process controlled by mass transport.

The current–time response is different when the potential is pulsed. After the potential E_1 is applied, the current

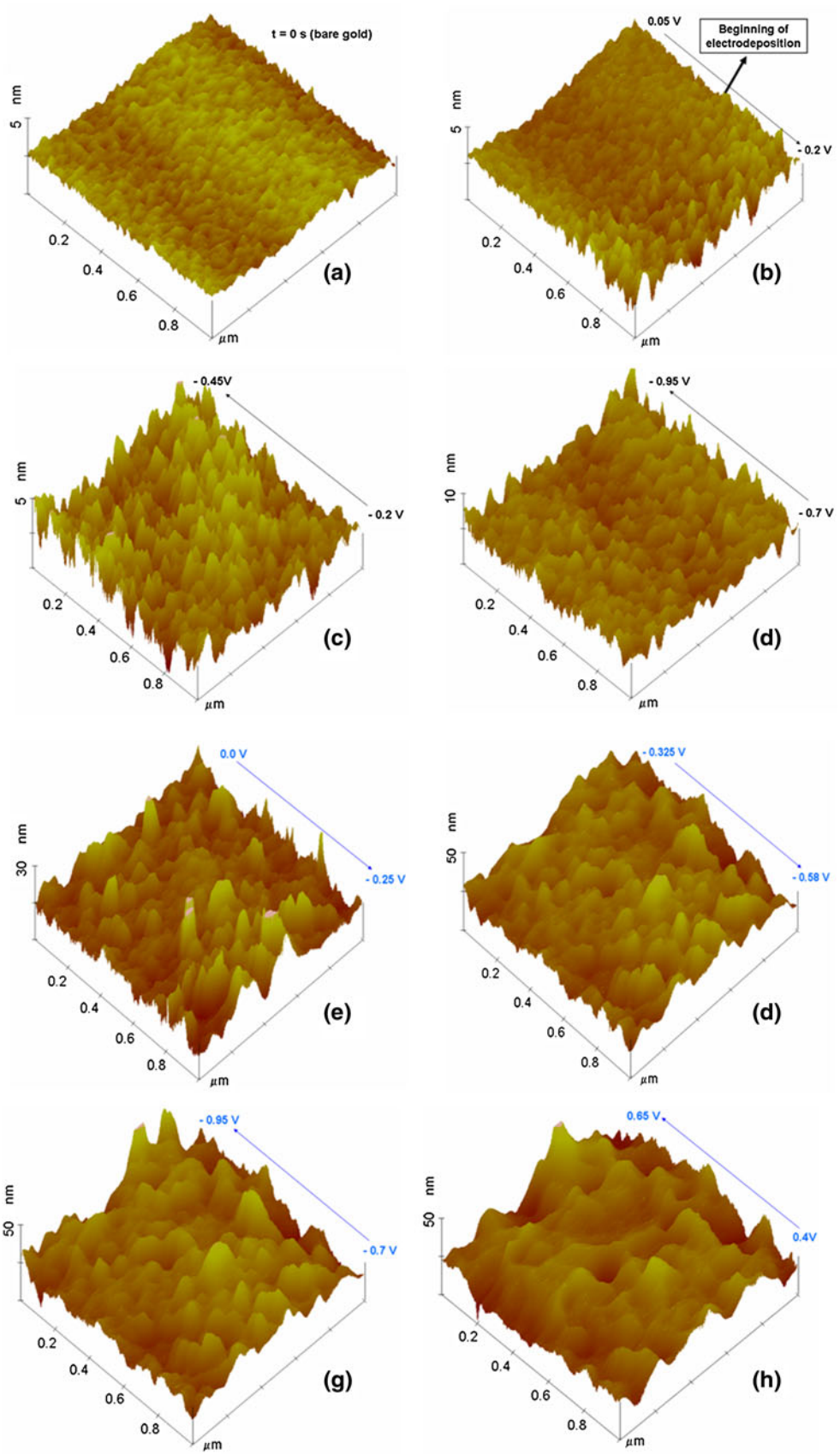

Fig. 2 In situ-AFM 3D images (1×1 µm) of a gold electrode in CISe precursor electrolyte. Each image corresponds to a potential range labeled in the CV being **a**–**e** for the first cycle and **f**–**h** for the second cycle. The *arrows* indicate the direction of the potential scan sweep

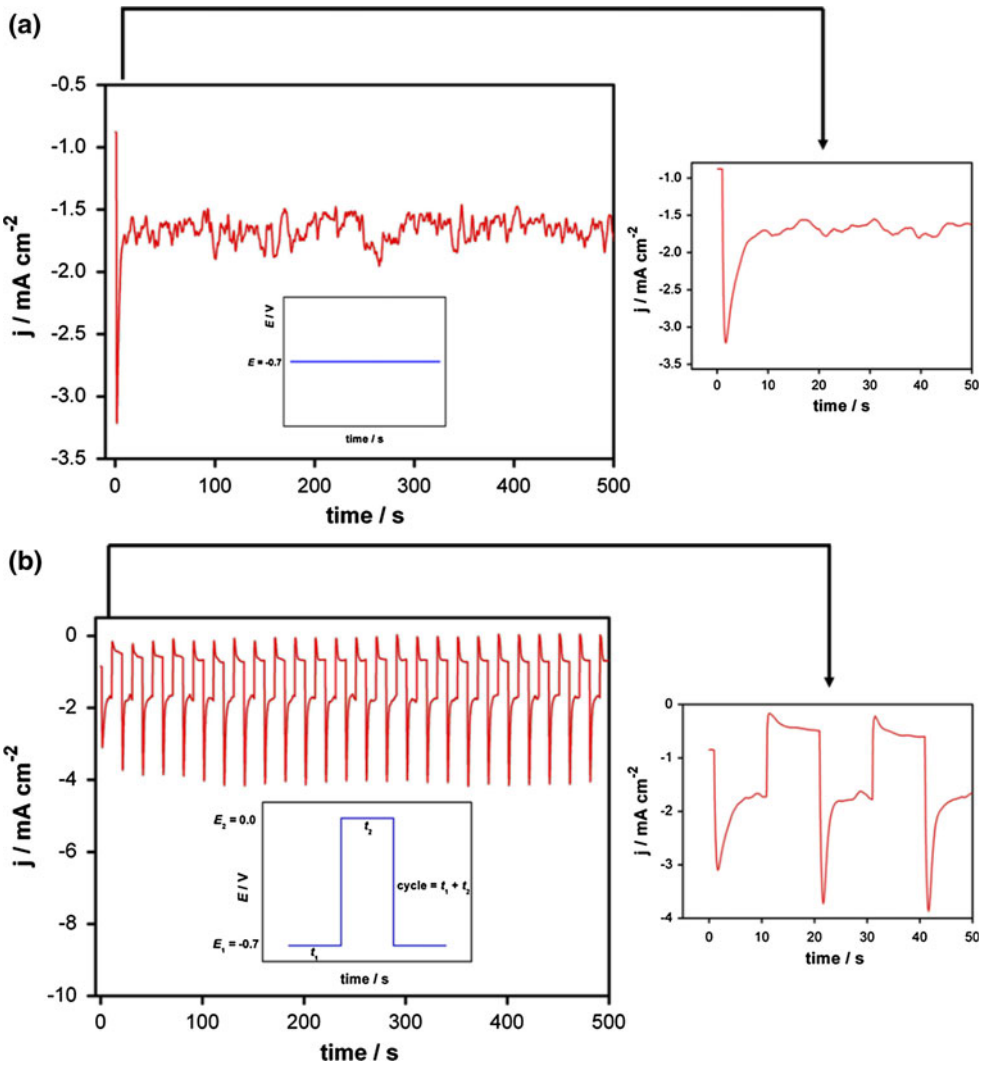

Fig. 3 Characteristic *J–t* response registered for **a** potentiostatic and **b** pulsed electrodeposition. The *inset* in each figure outlines the *E–t* profile imposed for each method, during the electrodeposition of $CuInSe_2$ films. Magnifications of the first 50 s are also provided to show in more detail the current pulse waveform

increases sharply and then decreases tending to a steady value as in potentiostatic mode. As potential E_2 is imposed, the current drops even more, reaching values close to zero. This is a so-called "relaxation period" that allows the diffusion of ions to areas where they have been quickly consumed while applying E_1. When a new pulse starts, the distribution of ions on the electrode surface is supposed to be more homogenous [22].

3.3 Characterization of electrodeposited CISe films

Figure 4 presents SEM images of as-deposited CISe films. Images (a) to (c) were obtained by pulsed electrodeposition with different E_1 potentials. At low potential values (−0.4 V) the morphology of the electrodeposited layer shows acicular shape agglomerated crystals. According to EDS results (see below) this morphology corresponds to Cu_xSe, taking into account that the indium content in the film is very low. Kois et al. [10] reported a similar film composition while studying the electrodeposition of CISe on Mo-glass substrates but using deposition potentials between −0.2 and −0.4 V (vs. SCE). They found very low In/Cu values in this potential window and they associated this behavior to a limited amount of CuSe previously deposited on the electrode, given that there is an insufficient supply of Se^{-2} ions to form In_2Se_3. This explanation could also be valid for pulsed electrodeposition but extended to more negative potentials (up to −0.5 V). At −0.5 V (Fig. 4b) two different kinds of particles seem to be present. This could indicate the coexistence of Cu_xSe and CISe, in agreement with Raman maps to be shown below. At potentials more negative than −0.5 V, the morphology is homogeneous again, but it changes into a cauliflower-like structure frequently found in electrodeposited CISe films [23–25]. At −0.6 V (not shown) and −0.7 V (Fig. 4c) a primary phase underneath, and a secondary phase dispersed on top of it, can be observed. This can be correlated to the incorporation of In(III) ions, which is favorable at more negative potentials, leading to a segregation of unreacted Cu_xSe compounds at the surface. In contrast to Fig. 4a–c, Fig. 4d shows the

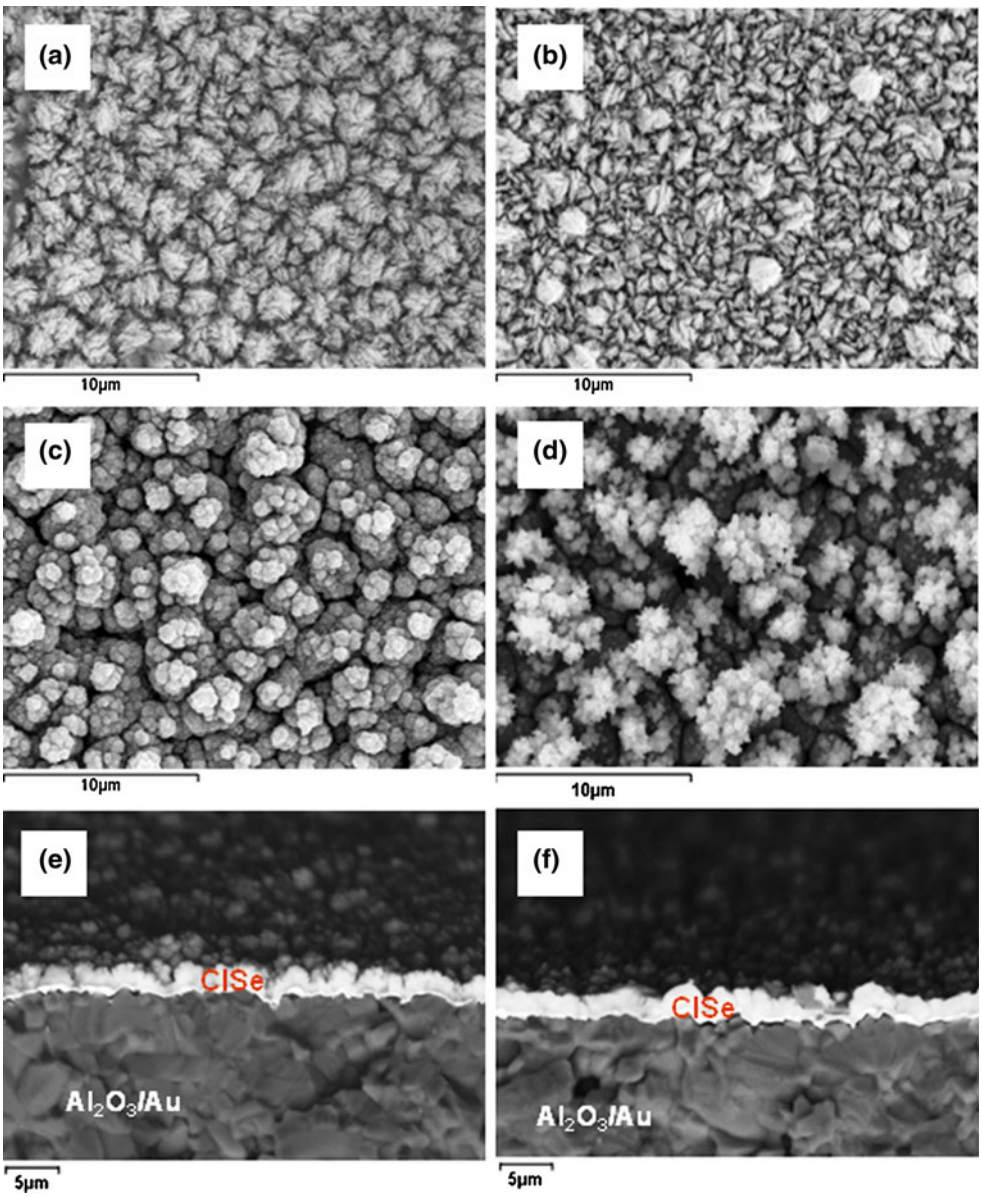

Fig. 4 SEM images of as-deposited CISe films on Al_2O_3/Au-coated substrates. **a**–**c** Films prepared by pulsed electrodeposition at different E_1 potentials **a** −0.4 V, **b** −0.5 V, **c** −0.7 V, **d** potentiostatic CISe films prepared at −0.7 V. **e**, **f** Cross-section images of the substrate/CISe interface for pulsed and potentiostatic CISe films obtained at −0.6 V. Average film thicknesses for pulse and potentiostatic CISe are 1.80 and 1.75 μm, respectively

morphology of a CISe film prepared at constant the potential (−0.7 V). In this case, potentiostatic electrodeposition results in more porous coral-like structures due to the enhancement of the diffusion-limited mass-transfer reactions that govern $CuInSe_2$ formation. Finally, cross-section SEM images are presented in Fig. 4e, f for both types of electrodeposited films. The layer thickness can be estimated in 1.80 and 1.75 μm for pulsed and potentiostatic films, respectively. These values are in good agreement with the thickness calculated using Faraday's law [14] for a total electrochemical charge of 4 C.

Figure 5 shows SEM images of selenized films. After a heat treatment in a Se-rich atmosphere, the morphology of the films deposited by pulsing the potential drastically changes, particularly in the case of those films prepared at the lower deposition potentials (compare Fig. 4a, b with Fig. 5a, b). Films deposited at more negative potentials (<−0.6 V) do not present significant changes in their morphology. This is also the case for the film obtained at a fixed potential (−0.7 V, Fig. 5d) which, after the selenization, retains the same morphology observed in the as-deposited film. All the films shown in Fig. 5 present a bilayered structure with a main phase at the bottom and a segregated secondary phase on top of it. The most compact and homogeneous morphology is observed for a pulsed electrodeposited film at −0.7 V (Fig. 5c).

Results showing the chemical composition obtained by EDS are presented in Fig. 6 for as-deposited pulsed and potentiostatic CISe films (Fig. 6a, b, respectively). In spite of the electrodeposition method (pulsed or potentiostatic) the copper content is always higher than the indium content. This is particularly true for pulsed films deposited at low E_1

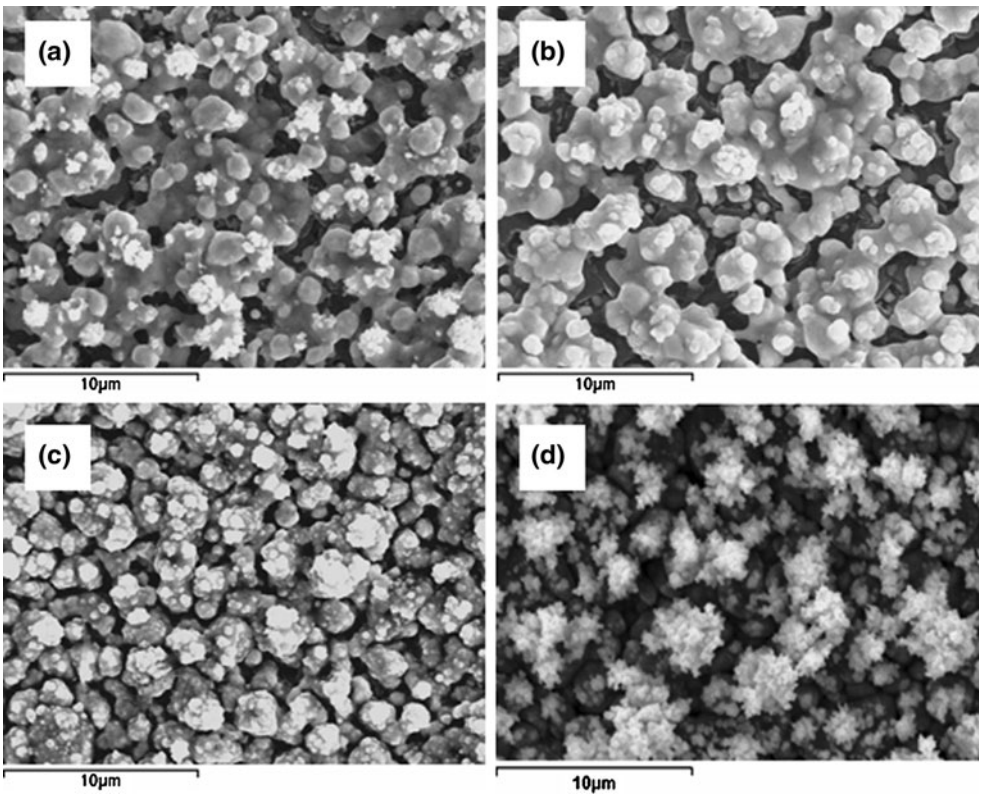

Fig. 5 SEM images of selenized CISe films on Al_2O_3/Au-coated substrates. **a**–**c** Films prepared by pulsed electrodeposition at different E_1 potentials **a** −0.4 V, **b** −0.5 V, **c** −0.7 V, **d** potentiostatic CISe films prepared at −0.7 V

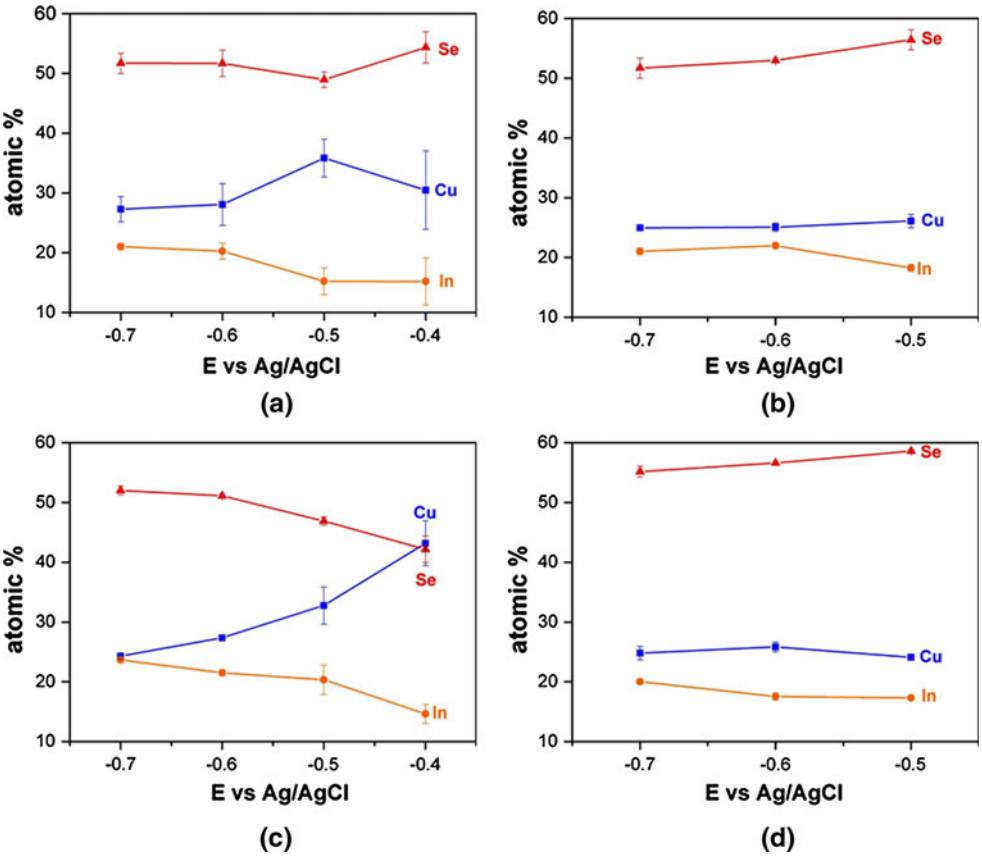

Fig. 6 Relationship between chemical composition and cathodic potential in as-deposited pulsed (**a**) and potentiostatic (**b**) electrodeposited CISe films. The change in the chemical composition after the selenization treatment is shown in **c**, **d** for pulsed and potentiostatic films, respectively

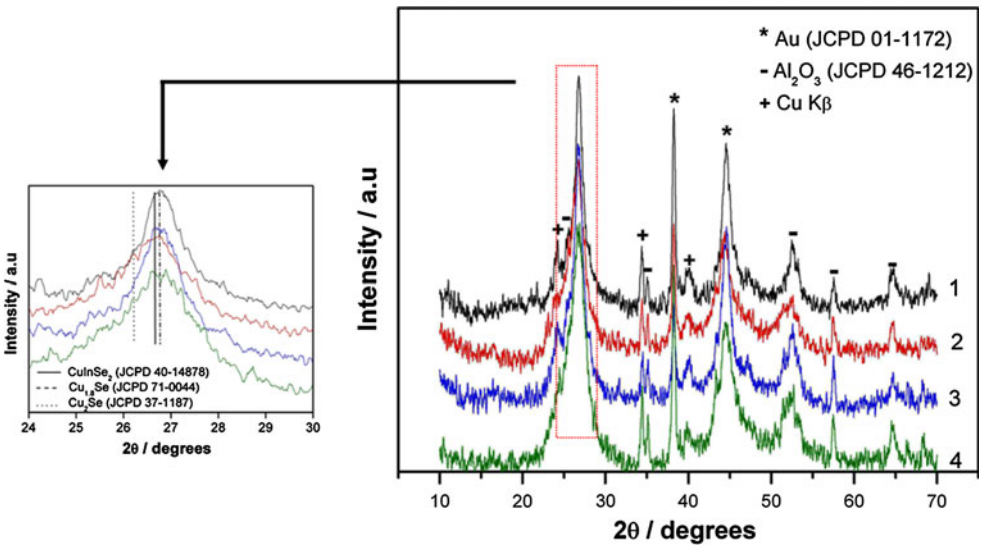

Fig. 7 GXRD of as-deposited CISe films. Different potential values and potential profiles are shown. (*1*) −0.5 V, pulsed; (*2*) −0.5 V, potentiostatic; (*3*) −0.7 V, pulsed; (*4*) −0.7 V, potentiostatic. The magnification shows in greater detail the main diffraction peak of CISe

potentials (−0.4 and −0.5 V) where the copper concentration exceeds 30 at.%. However, it should be noted that the composition value for the most positive potential shows the highest dispersion, given the more inhomogeneous nature of the film, as discussed above. This tendency for relatively high copper content could be indicating that copper deposition might be occurring during the "relaxation period" at 0.0 V (E_2). This is also seen in the AFM-cyclic voltammetry characterization (Fig. 1). At more negative E_1 potentials (−0.6 and −0.7 V) this would also occur but as more indium is incorporated to the film at these potentials, the copper deposition would be compensated.

On the other hand, potentiostatic films show more gradual changes with the applied potential. Lower potentials (−0.5 V) produce films highly rich in Se (close to 60 at.%). As it was observed for pulsed films, the indium content grows as the applied potential is set at more negative values. A nearly stoichiometric composition is obtained at −0.7 V. Figure 6c, d shows the chemical composition after the selenization treatment for pulsed and potentiostatic films, respectively. As it was observed as regards film morphology, the chemical composition in pulsed electrodeposited films is more dependent on the selenization treatment (Fig. 6c). At the most positive potentials, the copper content equals that of selenium in the film. This can be attributed to a prevalent crystallization of Cu_xSe during annealing. As the deposition potential becomes more negative, the chemical composition approaches the values of the stoichiometric formula. For instance, for a CISe film pulsed electrodeposited at −0.7 V and selenized, the composition results in $Cu_{0.24}In_{0.24}Se_{0.52}$.

Figure 7 presents GXRD diffractograms of as-deposited pulsed and potentiostatic CISe films. It can be seen that, even in grazing configuration, most of the peaks belong to the Al_2O_3/Au substrate or to unfiltered Cu-Kβ radiation of the X-rays beam. This can be related to the low crystallinity usually found in electrodeposited chalcopyrite thin films. Despite this, a broad signal between 25° and 28° is present in all the films. A zoom of this region allows the identification of different contributors to this peak, mainly binary Cu_xSe compounds and $CuInSe_2$.

As expected, the crystallinity of the film improves significantly after selenization, as can be seen in Fig. 8. It is clear that only after annealing the main diffraction planes from the CISe phase like (112), (204/220), and (116/312) dominate the diffractogram. The magnification shows again a zoom around the main diffraction peak (112) of CISe. It is clear that after selenization the center of the peak matches the position of the (112) plane of CISe and the contribution of secondary phases (Cu_xSe compounds) that was observed in as-deposited films is now absent. Moreover, is also evident that, after selenization, all peaks are sharper and narrower indicating an increment in the crystalline degree of the material.

It is known that Raman spectroscopy penetrates a few atomic layers and is more sensitive to changes close to the surface of the samples under analysis. Thus, it is very useful to avoid substrate interference, which is frequently found in XRD measurements. Raman maps are shown in Fig. 9 for CISe films deposited by pulsed and potentiostatic methods at different deposition potentials, before and after the selenization treatment. Raman spectra of $CuInSe_2$ films are characterized by a high intensity optical mode at 173–177 cm^{-1} known as A_1 mode [26, 27]. Raman spectra of as-deposited films (pulsed and potentiostatic) show a clear signal that corresponds to the A_1 main mode, indicating that the film is mainly composed by CISe. In particular, for the deposit obtained at −0.5 V by pulsed electrodeposition, additional modes are present in the

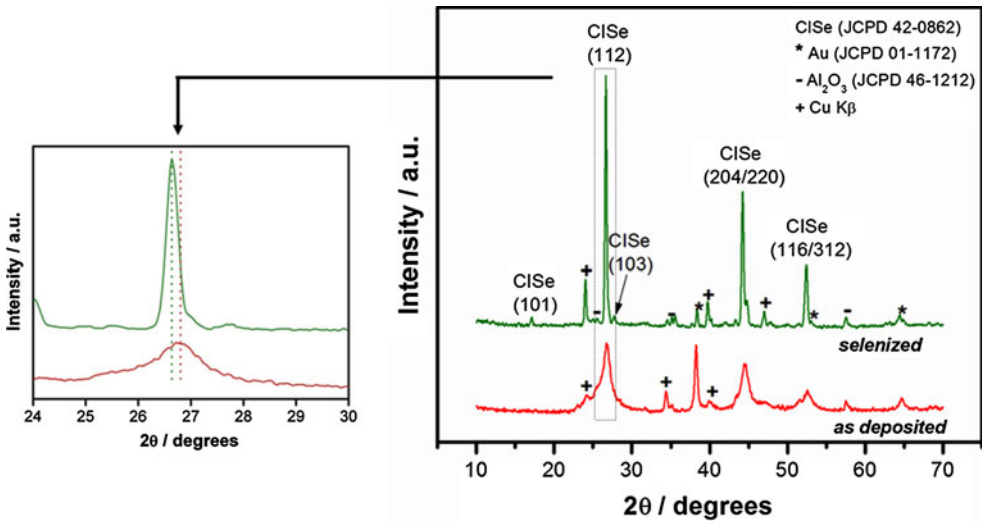

Fig. 8 GXRD diffractograms comparing as-deposited and selenized CISe films. Both films were obtained by pulsed electrodeposition (E_1: −0.7 V). The magnification shows in greater detail the (112) diffraction plane of CISe

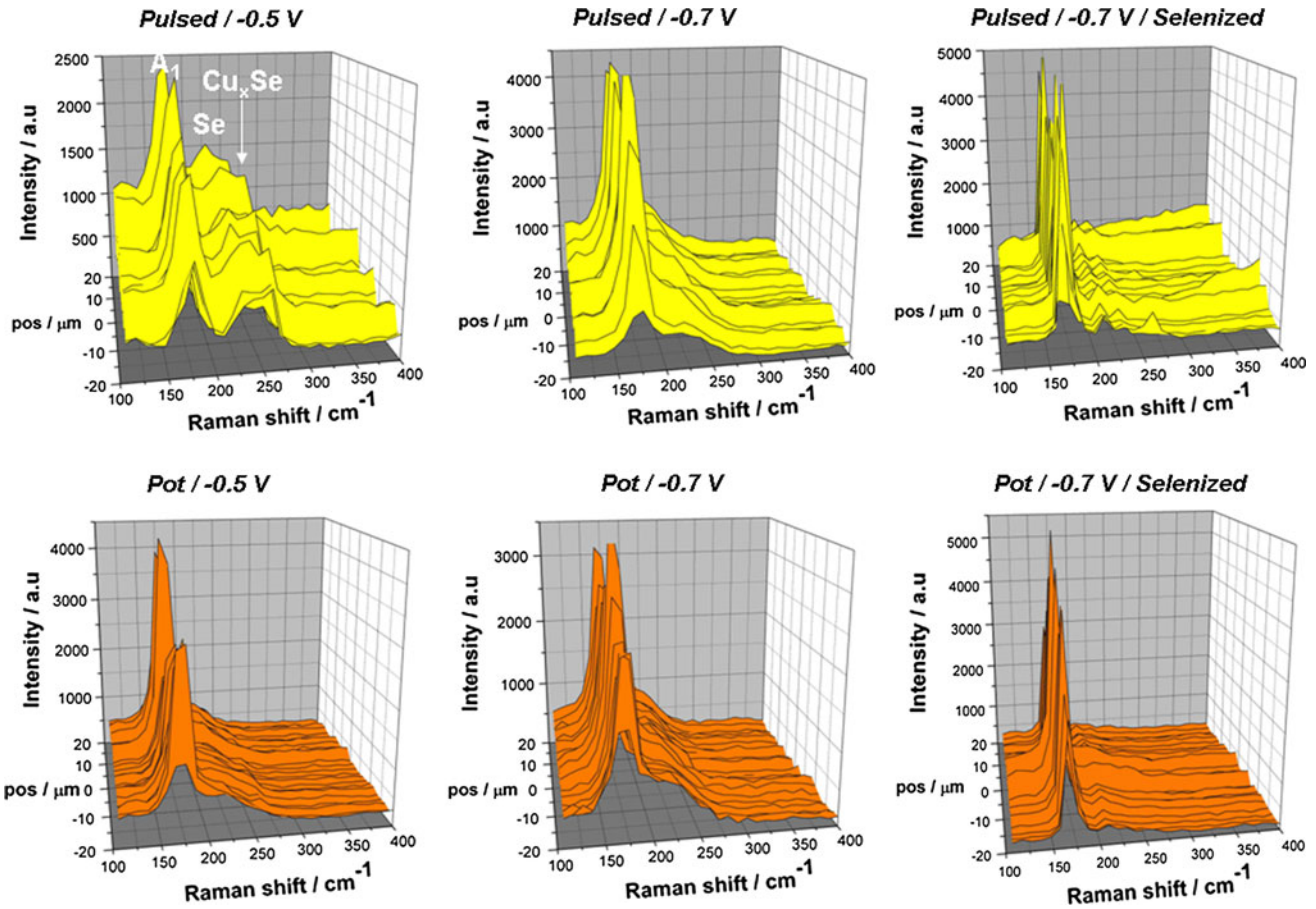

Fig. 9 Micro-Raman spectra comparing pulse and potentiostatic CISe films electrodeposited at different potentials. The influence of the selenization treatment is also shown

spectrum. First, an small lump around 235 cm^{-1} corresponding to a vibration mode of trigonal Se [28, 29] and a second shoulder between 250 and 260 cm^{-1} originate for Cu_xSe compounds present in the film [28, 30]. Raman spectra for CISe films deposited by pulsed electrodeposition are in good agreement with the chemical composition obtained by EDS analysis. Both techniques indicate that the most positive deposition potentials produce films highly rich in Cu and Se leading to the formation of Cu_xSe compounds. At more negative potentials the

signals typical of Se and Cu_xSe are no longer present in the Raman spectrum indicating that the film is mainly composed of $CuInSe_2$. After selenization, the A_1 mode of the CISe phase becomes sharper and intense, pointing out that the crystallinity of the films improved after the thermal treatment. Furthermore, two weak Raman signals at 206 and 215 cm^{-1} corresponding to $CuInSe_2$ vibration modes can be observed [26, 29]. Finally, it is worth pointing out that the composition of the selenized films is clearly homogeneous throughout the sample.

4 Conclusions

$CuInSe_2$ thin films were electrodeposited on gold-coated alumina electrodes using two different electrochemical approaches, potentiostatic and pulsed electrodeposition. The morphology and chemical composition of pulsed deposited CISe films were found to be highly sensitive to the deposition potential and the best stoichiometry is attained for films deposited at pulsed potentials of −0.7 V. In coincidence, the most compact and homogeneous morphology is observed for a pulsed electrodeposited film at −0.7 V.

In contrast, potentiostatic films presented minor variations in their chemical composition with the deposition potential. Potentiostatically grown films also present a more porous morphology.

In both cases a subsequent annealing in Se atmosphere is required to adjust the stoichiometry of the CISe films. Grazing incidence X-ray diffraction corroborates the presence of bigger coherent domains for electrodeposited CISe films after a thermal treatment at 500 °C in Se vapor. Raman spectroscopy and GXRD results show that the presence of secondary phases such as Cu_xSe and Se is drastically reduced after selenization. Raman maps confirm that the composition is homogenous throughout the whole sample.

Pulsing the potential during the electrodeposition has some advantages over keeping it constant. Using $E_1 = -0.7$ V and $E_2 = 0.0$ V a CISe film with larger grain size, a more compact surface morphology and the stoichiometric ratio could be obtained. The results obtained by pulsed electrodeposition are also more sensitive to the step potential limits.

Acknowledgments This study was partially supported by Spanish Government through MCINN grant MAT2009-14625-C03-03 and European Commission through NanoCIS project FP7-PEOPLE-2010-IRSES (ref. 269279). Financial support from Consejo Nacional de Investigaciones Científicas y Técnicas (CONICET), Agencia Nacional de Promoción Científica y Tecnológica and Universidad Nacional de Mar del Plata (UNMdP) from Argentina are greatly acknowledged. The authors wish to thank BSc. Mariela Desimone for her assistance with GXRD measurements.

References

1. Hibberd CJ, Chassaing E, Liu W et al (2010) Prog Photovolt Res Appl 18:434–452
2. Paunovic M, Schlesinger M (2006) Fundamentals of electrochemical deposition. The electrochemical society series. Wiley, Hoboken, New Jersey
3. Lincot D, Guillemoles JF, Taunier S et al (2004) Sol Energy 77(6):725–737
4. Arnulf J-W (2011) Sol Energy Mater Sol Cells 95(6):1509–1517
5. Whang TJ, Hsieh MT, Kao YC (2010) Appl Surf Sci 257(5):1457–1462
6. Hung P-K, Kuo T-W, Huang K-C et al (2012) Appl Surf Sci 258(18):7238–7243
7. Pandey RK, Sahu SN, Chanda S (1996) Handbook of semiconductor electrodeposition. Marcel Dekker, New York
8. Mishra KK, Rajeshwar K (1989) J Electroanal Chem 271(1–2): 279–294
9. Oliveira MCF, Azevedo M, Cunha A (2002) Thin Solid Films 405:129–134
10. Kois J, Bereznev S, Mellikov E et al (2006) Thin Solid Films 511–512:420–424
11. Ren T, Yu R, Zhong M et al (2011) Sol Energy Mater Sol Cells 95(2):510–520
12. Caballero-Briones F, Palacios-Padrós A, Sanz F (2011) Electrochim Acta 56(26):9556–9567
13. Hu SY, Lee WH, Chang SC et al (2011) J Electrochem Soc 158(5):B557–B561
14. Valdés MH, Vázquez M (2011) Electrochim Acta 56(19): 6866–6873
15. Valdés M, Vázquez M (2012) J Solid State Electrochem 16: 3825–3835
16. Kelley V, Serry M (2003) Electrochemical scanning probe microscopy manual version 5.30a. Veeco Instruments Inc. http://www.veeco.com/pdfs/user_Manuals/ElectroChemicalSPMB.pdf. Accessed 23 May 2003
17. International Centre for Diffraction Data (ICCD): Powder Diffraction File Database (1998) Newtown Square, EEUU
18. Samantilleke AP, Sahal M, Ortiz L et al (2011) Thin Solid Films 519(21):7272–7275
19. Calixto ME, Dobson KD, McCandless BE et al (2005) Growth mechanisms of electrodeposited $CuInSe_2$ and $Cu(In,Ga)Se_2$ determined by cyclic voltammetry. In: Materials Research Society Symposium Proceedings, pp 431–436
20. Breathnach M, Ahmed S, Nakahara S et al (2006) ECS Trans 1(11):25–39
21. Alvarez AE, Salinas DR (2010) Electrochim Acta 55(11): 3714–3720
22. Chandrasekar MS, Pushpavanam M (2008) Electrochim Acta 53(8):3313–3322
23. De Silva KTL, Priyantha WAA, Jayanetti JKDS et al (2001) Thin Solid Films 382(1–2):158–163
24. Araujo J, Ortíz R, López-Rivera A et al (2007) J Solid State Electrochem 11(3):407–412
25. Sene C, Calixto ME, Dobson KD et al (2008) Thin Solid Films 516(8):2188–2194
26. Rincón C, Ramírez FJ (1992) J Appl Phys 72(9):4321–4324
27. Izquierdo-Roca V, Pérez-Rodríguez A, Romano-Rodríguez A et al (2007) J Appl Phys 101:103517
28. Ramdani O, Guillemoles JF, Lincot D et al (2007) Thin Solid Films 515(15 SPEC. ISS.):5909–5912
29. Saucedo E, Ruiz CM, Chassaing E et al (2010) Thin Solid Films 518:3674–3679
30. Park JH, Yang IS, Cho HY (1994) Appl Phys Solid Surf 58(2): 125–128